

POLITECNICO DI TORINO  
Repository ISTITUZIONALE

Selective large-eddy simulation of hypersonic flows. Procedure to activate the filtering in unresolved regions only (arXiv:1211.1305, submitted to Computer Physics

*Original*

Selective large-eddy simulation of hypersonic flows. Procedure to activate the filtering in unresolved regions only (arXiv:1211.1305, submitted to Computer Physics Communications) / Tordella, Daniela; Iovieno, Michele; S., Massaglia; A., Mignone. - ELETTRONICO. - arXiv:1211.1305:(2012), pp. 1-12.

*Availability:*

This version is available at: 11583/2504243 since:

*Publisher:*

*Published*

DOI:

*Terms of use:*

This article is made available under terms and conditions as specified in the corresponding bibliographic description in the repository

*Publisher copyright*

(Article begins on next page)

# Selective large-eddy simulation of hypersonic flows. Procedure to activate the filtering in unresolved regions only.

D.Tordella<sup>a,\*</sup>, M.Iovieno<sup>a</sup>, S.Massaglia<sup>b</sup>, A.Mignone<sup>b</sup>

<sup>a</sup>Politecnico di Torino, Dipartimento di Ingegneria Meccanica e Aerospaziale, Corso Duca degli Abruzzi 24, 10129 Torino, Italy

<sup>b</sup>Università di Torino, Dipartimento di Fisica Generale, via P.Giuria 1, 10129 Torino, Italy

---

## Abstract

A new method for the localization of the regions where the turbulent fluctuations are unresolved is applied to the large-eddy simulation (LES) of a compressible turbulent jet with an initial Mach number equal to 5. The localization method used is called selective LES and is based on the exploitation of a scalar probe function  $f$  which represents the magnitude of the *stretching-tilting* term of the vorticity equation normalized with the enstrophy [1]. For a fully developed turbulent field of fluctuations, statistical analysis shows that the probability that  $f$  is larger than 2 is almost zero, and, for any given threshold, it is larger if the flow is under-resolved. By computing the spatial field of  $f$  in each instantaneous realization of the simulation it is possible to locate the regions where the magnitude of the normalized vortical stretching-tilting is anomalously high. The sub-grid model is then introduced into the governing equations in such regions only. The results of the selective LES simulation are compared with those of a standard LES, where the sub-grid terms are used in the whole domain. The comparison is carried out by assuming as reference field a higher resolution Euler simulation of the same jet. It is shown that the *selective* LES modifies the dynamic properties of the flow to a lesser extent with respect to the classical LES. In particular, the prediction of the enstrophy distribution and of the energy and density spectra are substantially improved.

*Keywords:* Small scale, Turbulence, Localization, Large-Eddy Simulation, Astrophysical Jets

*PACS:* 47.27.ep, 47.27.wg, 47.40.ki, 97.21.+a, 98.38.Fs

---

## 1. Introduction : the small scale detection criterion

Turbulent flows in many different physical and engineering applications have a Reynolds number so high that a direct numerical simulation of the Navier-Stokes equations (DNS) is not feasible. The large-eddy simulation (LES) is a method in which the large scales of turbulence only are directly solved while the effects of the small-scale motions are modelled. The mass, momentum and energy equations are filtered in space in order to obtain the governing equation for the large scale motions. The momentum and energy transport at the large-scale level due to the unresolved scales is represented by the so-called subgrid terms. Standard models for such terms, as, for example, the widely used Smagorinsky model, are based on the assumption that the unresolved scales are present in the whole domain and that turbulence is in equilibrium at subgrid scales (see, e.g., [2, 3]). This hypothesis can be questionable in free, transitional and highly compressible turbulent flows where subgrid scales, that is fluctuations on a scale smaller than the space filter size, are not simultaneously present in the whole domain. In such situ-

ations, subgrid models such as Smagorinsky's overestimate the energy flow toward subgrid scales and, from the point of view of the large, resolved, scales, they appear as over-dissipative by exceedingly damping the large-scale motion.

For instance, simulation of astrophysical jets could suffer from such limitation. In this regard, any improvement of the LES methodology is opportune. Astrophysical flows occur in very large sets of spatial scales and velocities, are highly compressible (Mach number up to  $10^2$ ) and have a Reynolds number which can exceed  $10^{13}$ , so that only the largest scales of the flow can be resolved even by the largest simulation in the foreseeable future. As a consequence, today, in this field, LES appears as a feasible simulation methods able to predict the unsteady system behaviour.

We have recently proposed a simple method to localize the regions where the flow is underresolved [1]. The criterion is based on the introduction of a local functional of vorticity and velocity gradients. The regions where the fluctuations are unresolved are located by means of the scalar probe function [1] which is based on the vortical stretching-tilting sensor:

$$f(\mathbf{u}, \boldsymbol{\omega}) = \frac{|(\boldsymbol{\omega} - \overline{\boldsymbol{\omega}}) \cdot \nabla(\mathbf{u} - \overline{\mathbf{u}})|}{|\boldsymbol{\omega} - \overline{\boldsymbol{\omega}}|^2} \quad (1)$$

where  $\mathbf{u}$  is the velocity vector,  $\boldsymbol{\omega} = \nabla \times \mathbf{u}$  is the vorticity vector and the overbar indicates the statistical average.

---

\*Corresponding author

Email address: daniela.tordella@polito.it (D.Tordella)

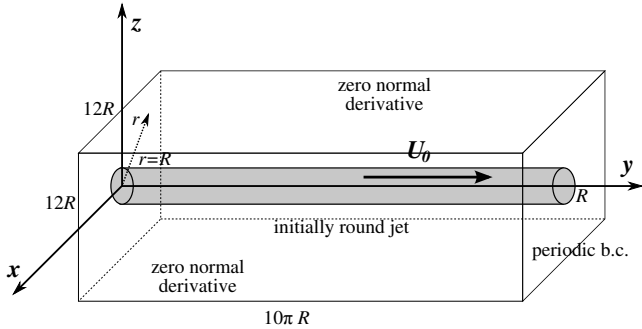


Figure 1: Scheme of the computational domain and boundary conditions. The initial condition is represented by the grey cylinder of radius  $R$ . The initial velocity field is a laminar parallel flow perturbed by eight waves which have an amplitude equal to 1% of the axis jet velocity and which has a wavelength from 1.25 to 10 times  $\pi R$ .

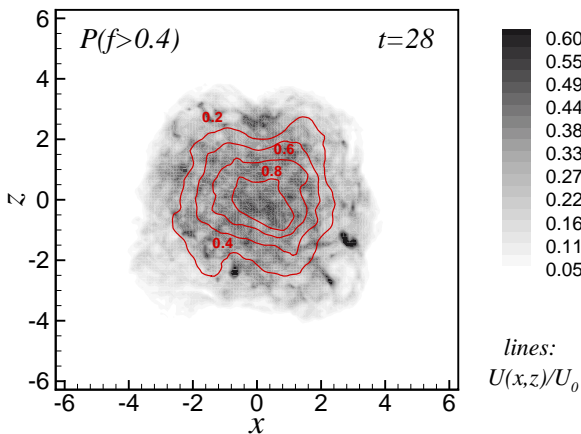


Figure 2: Contour plots at  $t = 28$  of the probability that  $f \geq t_\omega$  (see equation 1) and thus the probability that subgrid terms are introduced in the selective LES balance equation by the localization procedure. The lines represent the points where the longitudinal velocity  $\bar{u}/U_0$  is constant, where  $U_0$  is the jet axis mean velocity. All data in this figure have been computed averaging on lines parallel to the jet axis.

Function (1) is a normalized scalar form of the vortex-stretching term that represents the inertial generation of three dimensional vortical small scales inside the vorticity equation. When the flow is three dimensional and rich in small scales  $f$  is necessarily different from zero, while, on the other hand, it is instead equal to zero in a two-dimensional vortical flow where the vortical stretching is absent. The mean flow is subtracted from the velocity and vorticity fields in order to consider the fluctuating part of the field only.

A priori test of the spatial distribution of functional test have been performed by computing the statistical distribution of  $f$  in a fully resolved turbulent fluctuation field (DNS of a homogeneous and isotropic turbulent flow ( $1024^3$ ,  $Re_\lambda = 230$ , data from [4])) and in some unresolved instances obtained by filtering this DNS field on

coarser grids (from  $512^3$  to  $64^3$ ). It has been shown [1] that the probability that  $f$  assumes values larger than a given threshold  $t_\omega$  is always higher in the filtered fields and increases when the resolution is reduced. The difference between the probabilities in fully resolved and in filtered turbulence is maximum when  $t_\omega$  is in the range  $[0.4, 0.5]$  for all resolutions. In such a range the probability  $p(f \geq t_\omega)$  that  $f$  is larger than  $t_\omega$  in the less resolved field is about twice the probability in the DNS field. Furthermore, beyond this range this probability normalized over that of resolved DNS fields it is gradually increasing becoming infinitely larger. From that it is possible to introduce a threshold  $t_\omega$  on the values of  $f$ , such that, when  $f$  assumes larger values the field could be considered locally unresolved and should benefit from the local activation of the Large Eddy Simulation method (LES) by inserting a subgrid scale term in the motion equation. The values of this threshold is arbitrary, as there is no sharp cut, but it can be reasonably chosen as the one which gives the maximum difference between the probability  $p(f \geq t_\omega)$  in the resolved and unresolved fields. This leads to  $t_\omega \approx 0.4$ . Furthermore, it should be noted that the Morkovin hypothesis, stating that the compressibility effects do not have much influence on the turbulence dynamics, apart from varying the local fluid properties [5], allows to apply the same value of the threshold in compressible and incompressible flows.

Such value of the threshold has been used to investigate the presence of regions with anomalously high values of the functional  $f$ , by performing a set of a priori tests on existing Euler simulations of the temporal evolution of a perturbed cylindrical hypersonic light jet with an initial mach number equal to 5 and ten times lighter than the surrounding external ambient [1]. When the effect of the introduction of subgrid scale terms in the transport equation is extrapolated from those a priori tests, they positively compare with experimental results and show the convenience of the use of such a procedure [1, 6, 7].

In this paper we present large-eddy simulations of this temporal evolving jet, where the subgrid terms are selectively introduced in the transport equations by means of the local stretching criterion [1]. The aim is not to model a specific jet, but instead to understand, from a physical point of view, the differences introduced by the presence of subgrid terms in the underresolved simulations of hypersonic jets.

Our localization procedure selects the regions where subgrid terms are applied and, as such, its effect could be considered equivalent to a model coefficient modulation, as the one obtained by the dynamic procedure [8] or by the use of improved eddy viscosity Smagorinsky-like models like Vreman's model [9], which gives a low eddy viscosity in non turbulent regions of the flow. However, it operates differently because it is completely uncoupled from the subgrid scale model used as, unlike the common practical implementations of the dynamic procedure, does not require ensemble averaging to prevent unstable eddy vis-

cosity. Other alternatives, such as the approximate deconvolution model [10], are more complicated than the present selective procedure because involve filter inversion and the use of a dynamic relaxation term.

## 2. Flow configuration and numerical method

We have simulated the temporal evolution of a three dimensional jet in a parallelepiped domain with periodicity conditions along the longitudinal direction. The flow is governed by the fluid equations for mass, momentum, and energy conservation. In the astrophysical context, this formulation is usually considered to approximate the temporal evolution inside a spatial window of interstellar jets, which are highly compressible collimated jets characterized by Reynolds numbers of the order  $10^{13-15}$ . It is known that the numerical solution of a system of ideal conservation laws (such as the Euler equations) actually produces the equivalent solution of another modified system with additional diffusion terms. With the discretizations used in this study it possible to verify *a posteriori* that the numerical viscosity implies an actual Reynolds number of about  $10^3$ . In such a situation it is clear that the addition of the diffusive-dissipative terms into the governing equations would be meaningless. The formulation used is thus the following:

$$\begin{aligned} \frac{\partial \rho}{\partial t} + \frac{\partial}{\partial x_i}(\rho u_i) &= 0 \\ \frac{\partial(\rho u_k)}{\partial t} + \frac{\partial}{\partial x_i}(\rho u_i u_k + p \delta_{ik}) &= \frac{\partial}{\partial x_i} H(f_{\text{LES}} - t_\omega) \tau_{ik}^{\text{SGS}} \\ \frac{\partial E}{\partial t} + \frac{\partial}{\partial x_i}[(E + p)u_i] &= \frac{\partial}{\partial x_i} H(f_{\text{LES}} - t_\omega) q_i^{\text{SGS}} \end{aligned} \quad (2)$$

where the field variables  $p$ ,  $\rho$  and  $u_i$  and  $E$  are the filtered pressure, density, velocity, and total energy respectively. The ratio of specific heats  $\gamma$  is equal to  $5/3$ . Here  $\tau_{ik}^{\text{SGS}}$  and  $q_i^{\text{SGS}}$  are the subgrid stress tensor and total enthalpy flow, respectively. Function  $H(\cdot)$  is the Heaviside step function, thus the subgrid scale fluxes are applied only in the regions where  $f > t_\omega$ . The threshold  $t_\omega$  is here taken equal to 0.4, which is the value for which the maximum difference between the probability density function  $p(f > t_\omega)$  between the filtered and unfiltered turbulence was observed [1]. Sensor  $f$ , as defined in (1), does not depend on the subgrid model used and on the kind of discretization used to actually solve the filtered transport equations. In principle, it can be coupled with any subgrid model and any numerical scheme. We have chosen to implement the standard Smagorinsky model as subgrid model,

$$\begin{aligned} \tau_{ij}^{\text{SGS}} + \frac{1}{3} \tau_{kk}^{\text{SGS}} &= \rho \nu_\delta S_{ij}, \quad \nu_\delta = (C_s \delta)^2 |S| \\ q_i^{\text{SGS}} &= \rho \frac{\nu_\delta}{Pr_t} \frac{\partial}{\partial x_i} E \end{aligned}$$

where  $S_{ij}$  is the rate of strain tensor and  $|S|$  its norm. Constant  $C_s$  has been set equal to 0.1, which is the standard value used in the LES of shear flows, and  $Pr_t$ , the

turbulent Prandtl number, is taken equal to 1. The initial flow configuration is an axially symmetric cylindrical jet in a parallelepiped domain, described by a cartesian coordinate system  $(x, y, z)$ . The initial jet velocity is along the  $y$ -direction; its symmetry axis is defined by  $(x = 0, z = 0)$ . The interface between the jet and the surrounding ambient medium is described by a smooth velocity and density transition in order to avoid the spurious oscillations that can be introduced by a sharp discontinuity. The flow profile is thus initialized as

$$\bar{u}(r) = \frac{U_0}{\cosh(r/a)^m}$$

where  $r^2 = x^2 + z^2$  is the distance from the jet axis,  $R$  is the jet radius and  $U_0$  the jet velocity.  $m$  is a smoothing parameter which has been set equal to 4. The same smoothing has been used for the initial density distribution,

$$\bar{\rho}(r) = \rho_0 \left( \nu - \frac{\nu - 1}{\cosh(r/a)^m} \right)$$

where  $\rho_0$  is the density of the external ambient and  $\nu$  is the ratio between the jet density and  $\rho_0$ . A value of  $\nu$  larger than one implies that the jet is lighter than the external medium. The mean pressure is set to a uniform value  $p_0$ , that is, we are considering a situation where there is initially a pressure equilibrium between the jet and the surrounding environment. This initial mean profile is perturbed at  $t = 0$  by adding longitudinal transversal velocity disturbances whose amplitude is 1% of the jet velocity and whose wavelength is up to eight times the fundamental wavelength  $2\pi/R$ ,

$$u_i(x, y, z) = \frac{1}{100} U_0 \sum_{n=0}^8 \sin \left( n \frac{2\pi}{L_y} y + \varphi_n \right)$$

with  $\varphi_n$  random phase shifts, so that even the perturbation with the shortest wavelength is, initially, fully resolved. The integration domain is  $-L_x \leq x \leq L_x$ ,  $0 \leq y \leq L_y$  and  $-L_x \leq z \leq L_x$ , with  $L_x = 6R$  and  $L_y = 10\pi R$ . We have used periodic boundary conditions in the longitudinal  $y$  direction, while zero normal derivative outflow conditions are used for all variables in the other directions. A scheme of the initial flow configuration used in the simulations is shown in figure 1.

In the following, all data have been made dimensionless by expressing lengths in units of the initial jet radius  $R$ , times in units of the sound crossing time of the radius  $R/c_0$ , where  $c_0 = \sqrt{\gamma p_0/\rho_0}$  is the reference sound velocity of the initial conditions, velocities in units of  $c_0$  (thus dimensionless velocities coincide with the initial Mach number), densities in units of  $\rho_0$  and pressures in units of  $p_0$ .

Equations (2-4) have been solved, in Cartesian geometry, using an extension of the PLUTO code [12], which is a Godunov-type code that supplies a series of high-resolution shock-capturing schemes [13] that are particularly suitable for the present application, because of their

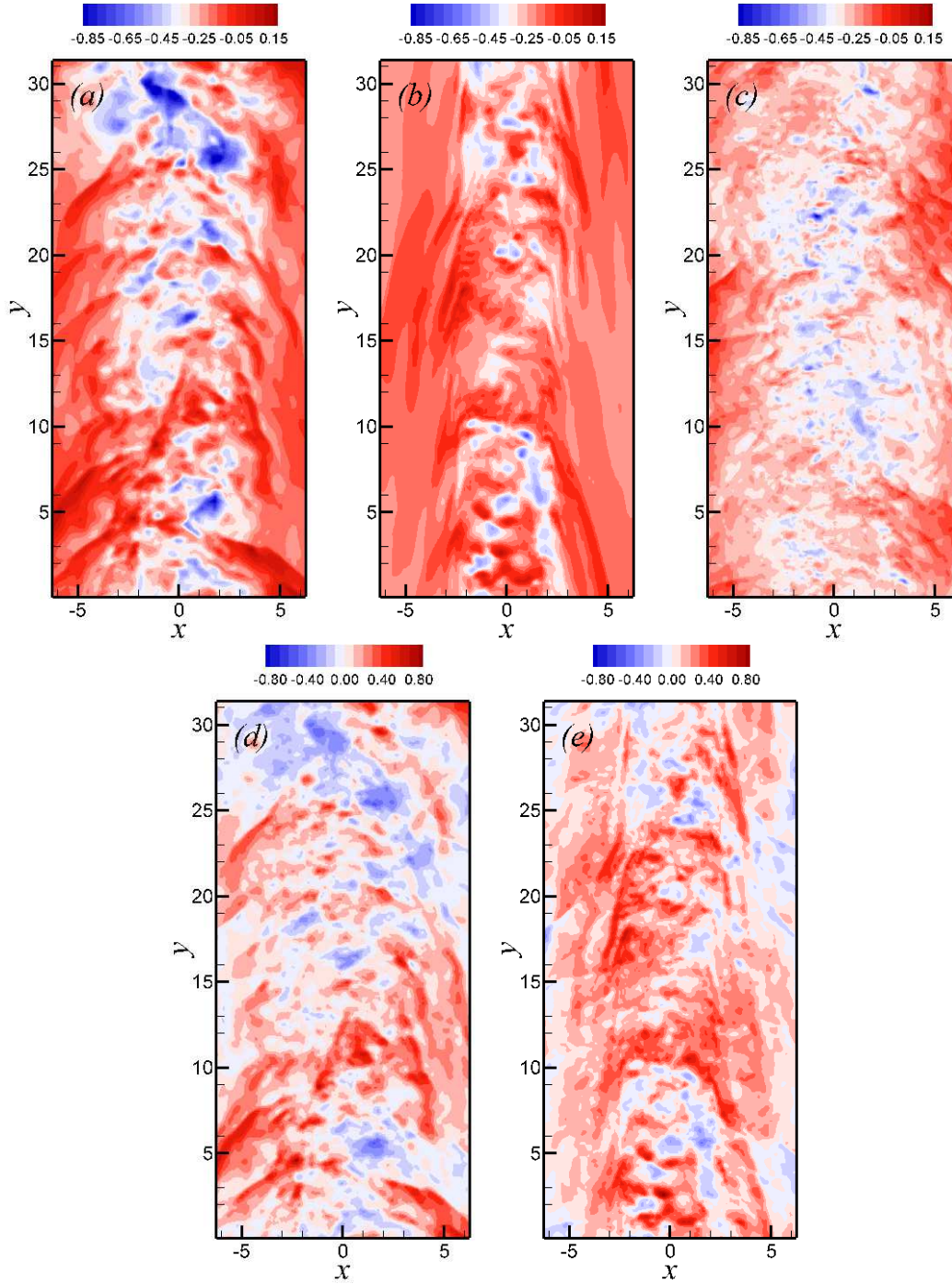


Figure 3: ((a), (b), (c)): Pressure distribution in a longitudinal section at  $t = 32$ : (a) selective LES, (b) standard LES, (c) higher resolution pseudo-DNS. The figures show the contour levels of  $\log_{10}(p/p_0)$ , the mean flow is from bottom to top. ((d), (e)): Local difference between the LES pressure fields and the higher resolution pseudo-DNS at  $t/\tau = 32$ : (d) selective LES, (e) standard LES. The figures show the contour levels of  $(p_{LES} - p_{DNS})/p_0$ .



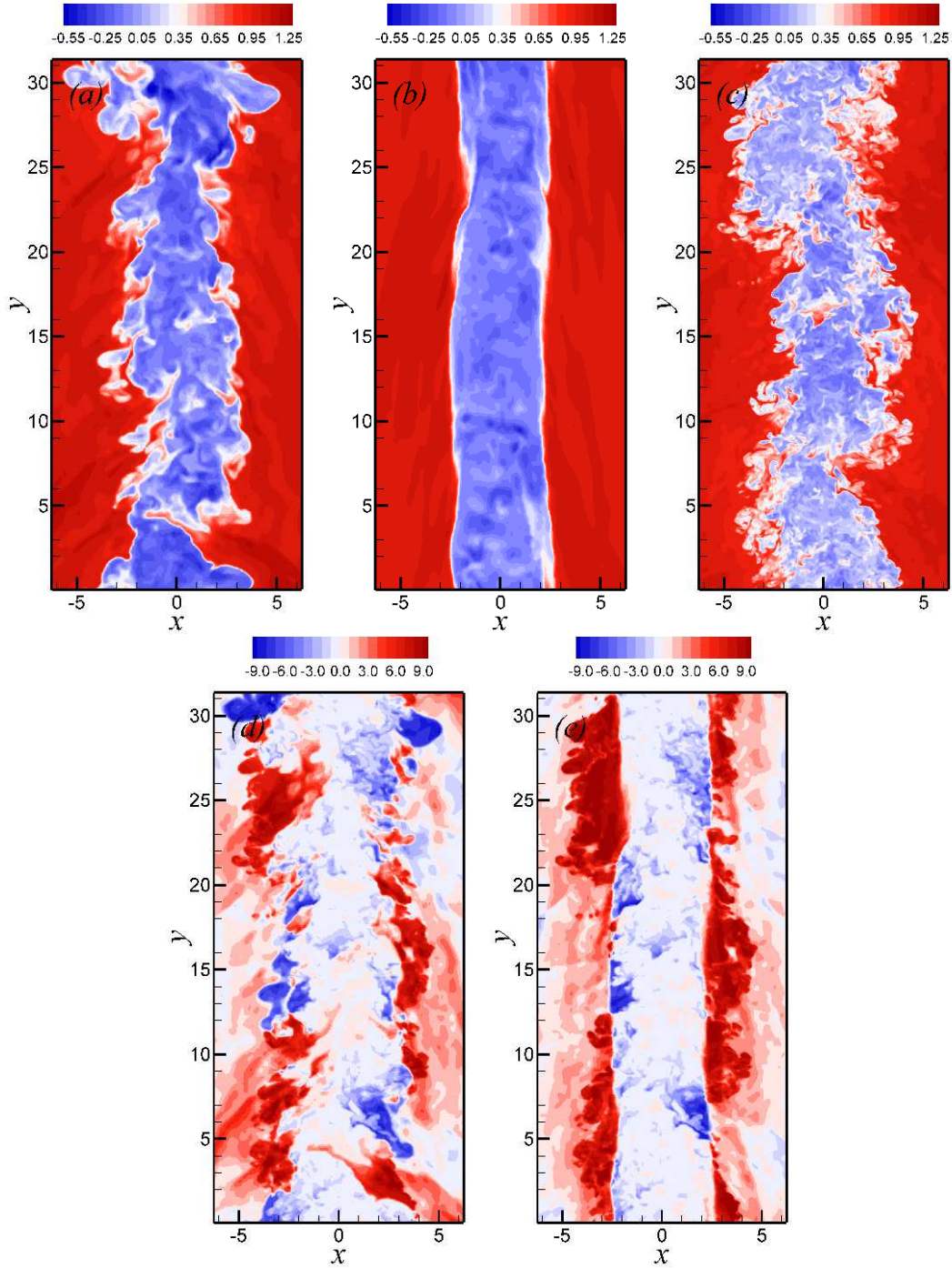


Figure 4: ((a), (b), (c)): Density variation in a longitudinal section at  $t = 32$ : (a) selective LES, (b) standard LES, (c) higher resolution pseudo-DNS. The figures show the contour levels of  $\log_{10}(\rho/\rho_0)$ , the mean flow is from bottom to top. ((d), (e)): Local difference between the LES density fields and the higher resolution pseudo-DNS at  $t/\tau = 32$ : (d) selective LES, (e) standard LES. The figures show the contour levels of  $(\rho_{LES} - \rho_{DNS})/\rho_0$ .

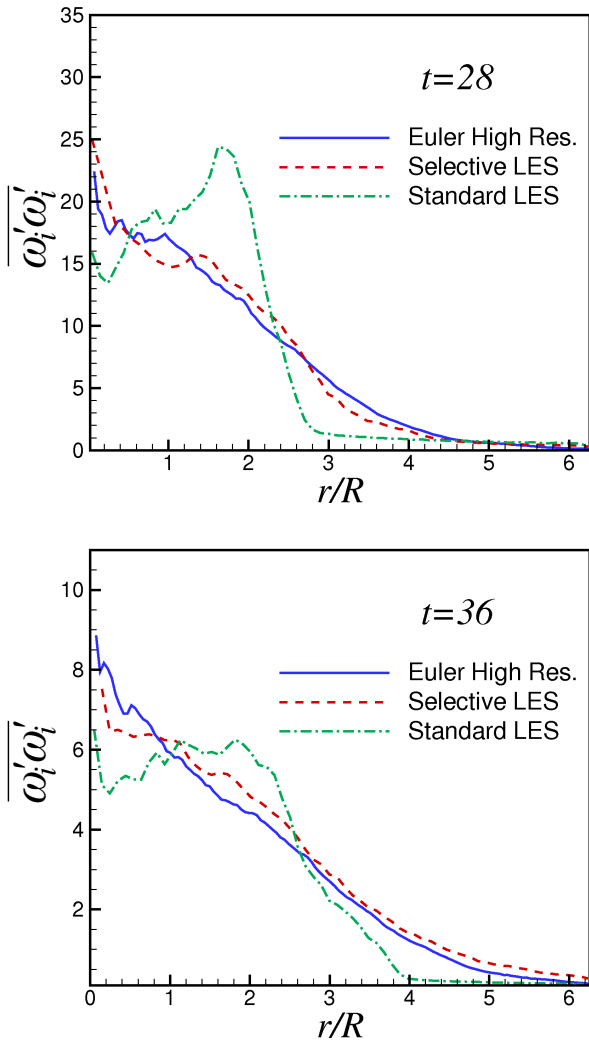


Figure 5: Radial distribution of the enstrophy  $\overline{\omega'_i \omega'_i}$  as function of the distance  $r$  from the axis of the jet. All averages have been computed as space averages on cylinders at constant  $r = 2$ .

low numerical dissipation. In fact, as pointed out by [14], a high numerical viscosity can overwhelm the subgrid-scale terms effects. The code has been extended by adding the subgrid fluxes and the computation of the functional  $f$  which allows to perform the selective large-eddy simulation. For this application, a third order accurate in space and second order in time Piecewise-Parabolic-Method (PPM) has been chosen.

We have performed three simulations of a jet with an initial Mach number equal to 5 and a density ratio  $\nu$  equal to 10. The density ratio is an important parameter in such flow configuration, as it has been shown that it has a strong influence on the temporal evolution and on the flow entrainment as it has been shown by numerical simulations and laboratory experiments [17]. The selective LES of the jet has been carried out on a  $320 \times 128^2$  uniform grid. Moreover, two additional simulations were performed for comparison: a standard non selective LES where the sub-

grid model was introduced in the whole domain, which is obtained by forcing  $H \equiv 1$  in equations (2-4), and a higher resolution ( $640 \times 256^2$ ) Euler simulation, which formally can be obtained by putting  $H \equiv 0$ .

### 3. Results

In this configuration we follow the evolution of a compressible jet from the amplification of a few unstable modes to the final quasi-steady turbulent state. As it is known from previous study on the subject (e.g.[16]), four main stages can be identified in the temporal evolution of hypersonic jet. In the first phase, the unstable modes introduced by the perturbations grow up in agreement to the linear theory till their growth leads to the formation of internal shocks. This stage is followed by a second phase where the jet is globally deformed and shocks are driven in the external medium, thus carrying momentum and energy away from the jet and transferring them to the external ambient. At this point a so called mixing stage occurs: as a consequence of the shock evolution, mixing between the jet and external material begins to occur. The longitudinal momentum, initially concentrated inside the jet radius, is spread over a much larger region by the mixing of the jet material. In the end the jet reaches a statistically quasi-stationary phase and slowly decays.

The mixing phase where the flow can be considered turbulent, is reached after about 15 initial sound crossing times. At this point, the resolution could not be enough to solve all the scales and, consequently, the momentum and energy transport due to presence of subgrid scales, should be introduced: the subgrid terms must be active in the underresolved regions. Figure 2 shows, in our selective large-eddy simulation, the probability that the sensor  $f$  is larger than the threshold, that is, that subgrid scales are present, at  $t = 28$ . At this stage about 40-60% of the jet is underresolved and subgrid terms are applied in such zones. At the same time, the external ambient is still resolved with the LES grid.

The effect of the subgrid scale terms can be qualitatively appreciated in the visualizations of the pressure and density fields. A visualization of the pressure field in a longitudinal section at  $t = 32$  is shown in figure 3(a-c) for the three simulations (selective LES, classical LES, high resolution Euler simulation). The comparison shows the larger dissipation and the small scale suppression produced by the non selective use of the subgrid model in the whole domain. This is even more evident in the plot of the density field (figure 4(a-c)): subgrid terms used in the whole volume of flow tend to delay the mixing of the jet and reduce the spreading of the jet material. Parts (d) and (e) of figure 3 and 4 present the difference between the pressure and densities predicted, at  $t = 32$ , by the LES methods and the higher resolution pseudo-DNS. The selective LES mainly introduces, in comparison with the higher resolution simulation, a shift on the pressure/density fluctuations in the longitudinal direction, while the standard

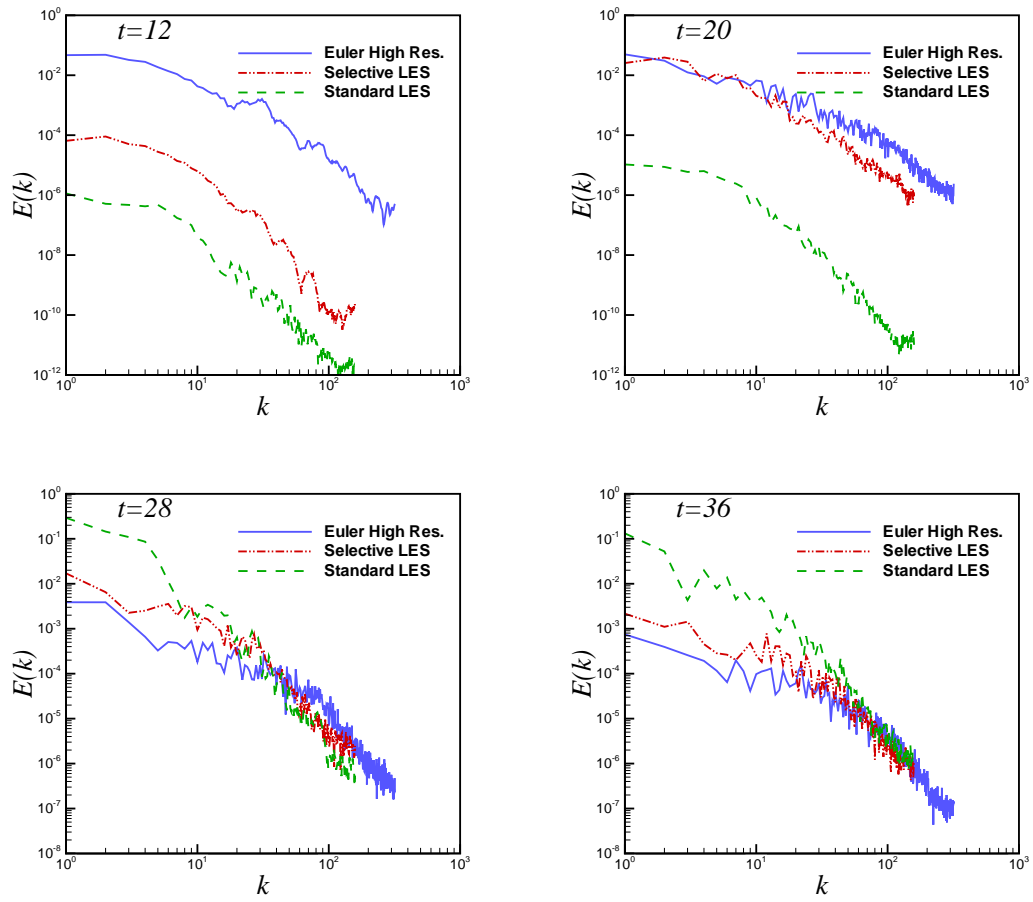


Figure 6: Longitudinal one dimensional spectra of the turbulent kinetic energy obtained by considering all data on the cylindrical surface at  $r = 2$ , computed as the Fourier transform of the two-point correlations of the fluctuating kinetic energy  $\rho u_i^2/2$ .



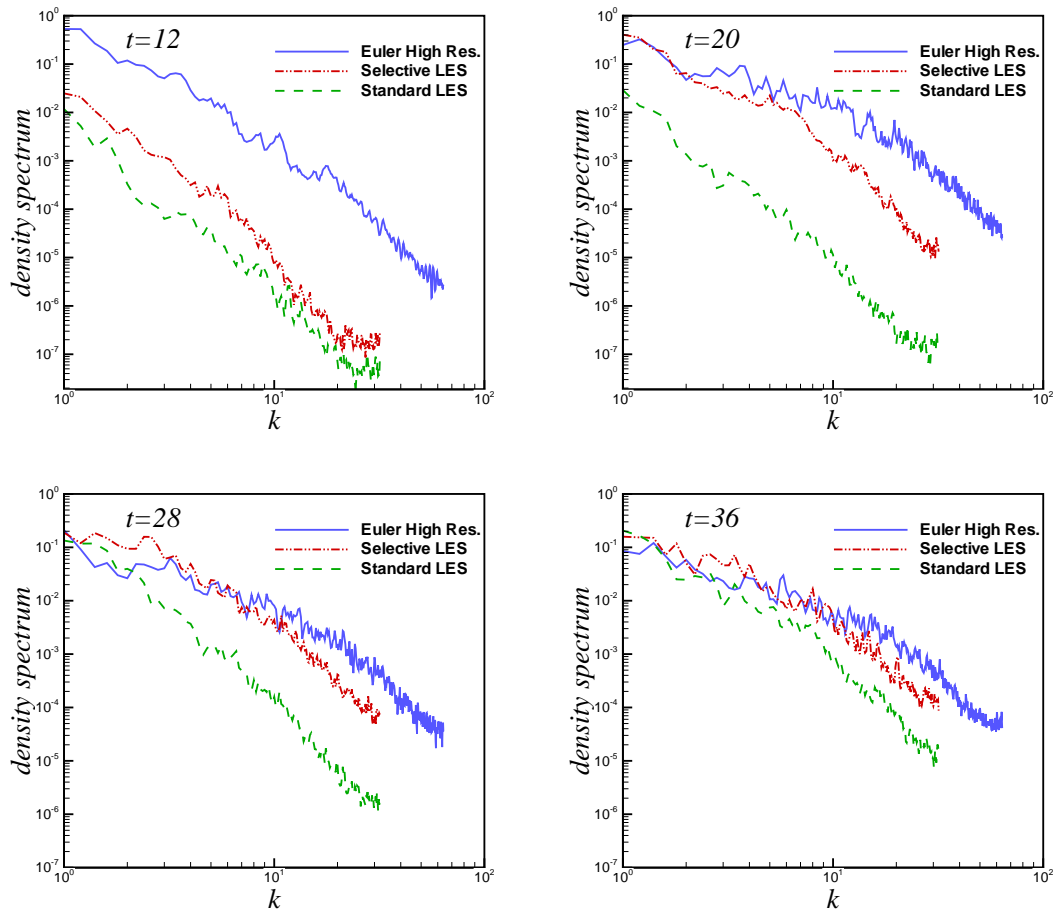


Figure 7: Longitudinal one dimensional spectra of the density fluctuations obtained by considering all data at a distance from the jet axis equal to  $r = 2$ .

LES mainly tends to suppress the density fluctuations at the jet border and thus reduces the flow entrainment.

The time evolution of the enstrophy distribution at two time instants far from the initial one is shown in figure 5 as a function of the distance from the centre of the jet. While the agreement between the enstrophy distribution obtained with the selective LES simulation and with the reference high resolution Euler simulation is fair, the non selective simulation damps out the vorticity magnitude in the center of the jet and in the outer part, and introduces a spurious accumulation in the intermediate radial region. As a results, the vorticity dynamics is highly modified. The overall effect is a delay in the formation of the turbulent structures, as it is evident when the spectrum of the turbulent kinetic energy is considered. Figure 6 and figure 7 show the one dimensional longitudinal kinetic energy and the fluctuating density spectra at  $r = 2$ , that is in the intermittent region between the jet core and the surrounding ambient. All spectra have been computed by averaging on points at the same distance from the jet axis. It can be noted that, in the non selective LES, the growth of fluctuations is much slower and, as a consequence, they have much less energy in the first stage of evolution. Moreover, even when the energy of the fluctuations in the non selective LES reaches levels comparable with those of both the selective LES and the higher resolution run ( $t = 28$  and  $36$ ), there is a significant concentration of energy in the low wavenumber region, which becomes even more pronounced in the later stages ( $t = 36$ ). This is consistent with the higher level of enstrophy seen in figure 5 for the non selective LES at a similar distances from the centre of the jet. Thus, we can observe that the selective introduction of the subgrid model yields spectral distributions of the energy much closer, with respect to the standard LES, to the distribution shown by the high resolution Euler simulation.

A more quantitative assessment of the impact of the different modelling procedures on the overall flow features can be made by considering the mean quantities, in particular the velocity longitudinal distribution and the jet thickness. The mean velocity profiles are shown in figure 8. It is possible to appreciate not only the different temporal decay of the axial velocity but also the different shapes of the velocity profiles for the three simulations: the standard LES has a slower decay of the velocity on the jet axis and, in general, overall steeper profiles of both mean velocity and mean density (see figures 8 and 9). To evaluate the spreading rate of the jet, we consider the geometrical thickness  $\delta$  of the velocity profiles, here defined as the distance from the jet axis where  $\bar{u}/U_0 = 0.5$ , and the geometrical thickness  $\delta_\rho$  of the density profiles, defined as the distance from the jet axis where  $\bar{\rho} = (\bar{\rho}(0) + \bar{\rho}(\infty))/2$ . While the geometrical velocity thickness  $\delta$  does not seem to show a high sensitivity to the flow modelling, the density thickness clearly indicates the delay in the growth of the standard LES, which produces a reduced entrainment.

The temporal growth rate of the jet thickness can be

transformed in an equivalent spatial growth rate by means of the Taylor transformation  $x = U_0 t$ , that is,

$$\frac{d\delta}{dx} = \frac{1}{U_0} \frac{d\delta}{dt}.$$

In the first part of the simulation, up to  $t = 15$ , both thickness grow very slowly. In this stage there the initial perturbations are still growing [16] and the mixing between the jet and external material is not yet begun. Both the higher resolution simulation and the selective LES present, in the second part of the simulation, an equivalent spatial growth rate equal to about 0.028. Even if the selective LES growth begins with a small delay, it presents almost the same growth rate. Such value is in line with what can be expected in such a flow [1, 7]. The large delay in the growth of turbulence structures induced by the standard non selective LES, which is visible in the velocity and density spectra (see figures 6 and 7), is clearly evident also in the jet thickness, which presents also a lower growth rate. This delay can be attributed to the overestimation of unresolved subgrid scales transport made by the standard non selective LES model, which leads to an initial damping of the resolved large scale structures which are mainly responsible for the jet entrainment.

#### 4. Concluding remarks

In this work we show that the *selective* Large Eddy Simulation, which is based on the use of a scalar probe function  $f$  – a function of the magnitude of the local stretching-tilting term of the vorticity equation – can be conveniently applied to the simulation of time evolving compressible jets. In the present simulation, the probe function  $f$  has been coupled with the standard Smagorinsky sub-grid model. However, it should be noted that the probe function  $f$  can be used together with any model because  $f$  simply acts as an independent switch for the introduction of a sub-grid model. The main results is that even a simple model can give acceptable results when selectively used together with a sub-grid scale localization procedure. In fact, the comparison among the three kinds of simulation (selective LES, standard LES, high resolution pseudo Euler direct numerical simulation) here carried out shows that this method can improve the dynamical properties of the simulated field. In particular, the selective LES improves the spectral distribution of the energy and density over the resolved scales, the enstrophy radial distribution and the mean velocity and density profiles. Furthermore, this method avoids the artificial over-damping of the unstable modes at the jet border which in the standard large eddy simulation inhibits the jet lateral growth. Because of this properties, given the modest computational burden brought to the simulation, the application of the selective procedure to the simulation of complex flows - in particular highly compressible free flows as, for instance, astrophysical jets - seems promising.

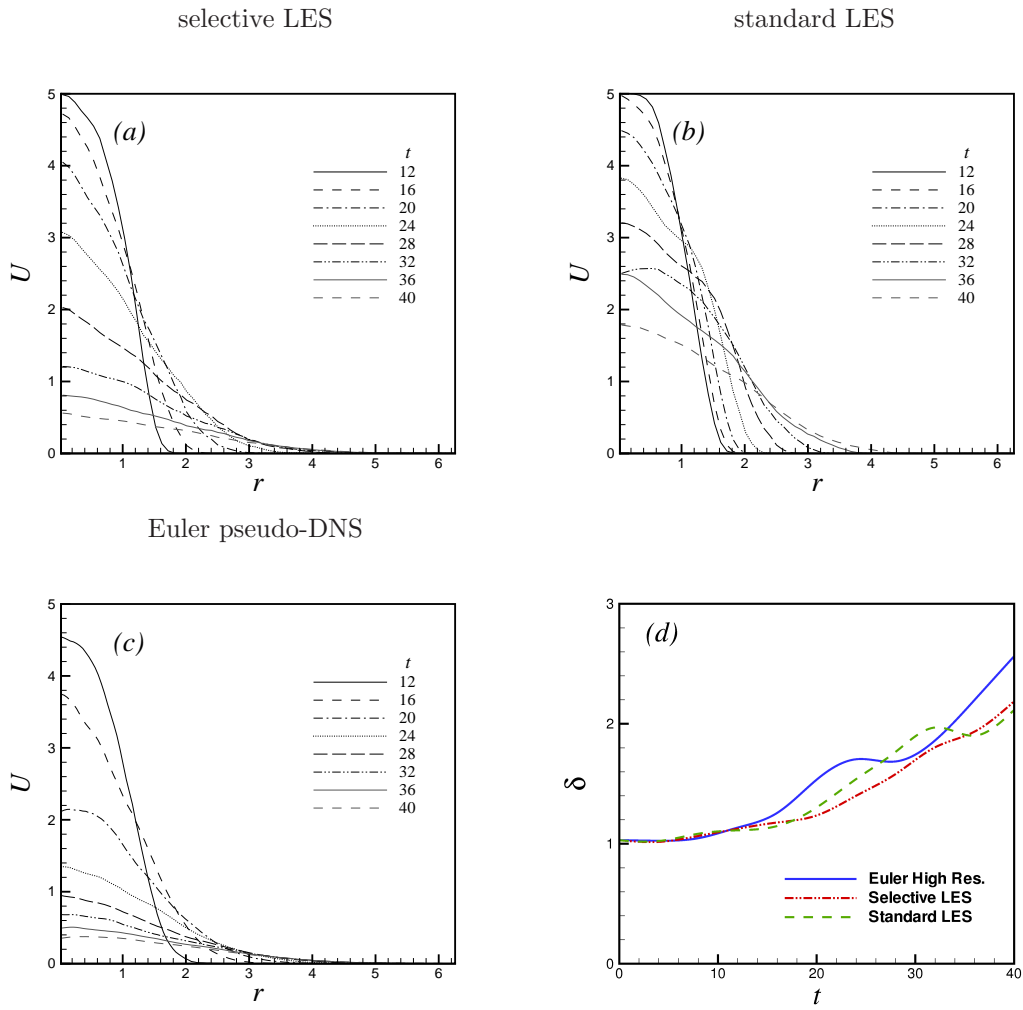


Figure 8: ((a),(b),(c)): Mean velocity profiles at different instants: (a) mean density, selective LES; (b) mean density, standard LES; (c) mean density, high resolution simulation. (d) time evolution of the geometrical thickness  $\delta$ , defined as the distance from the jet axis where  $U/U_0$  is equal to 0.5.

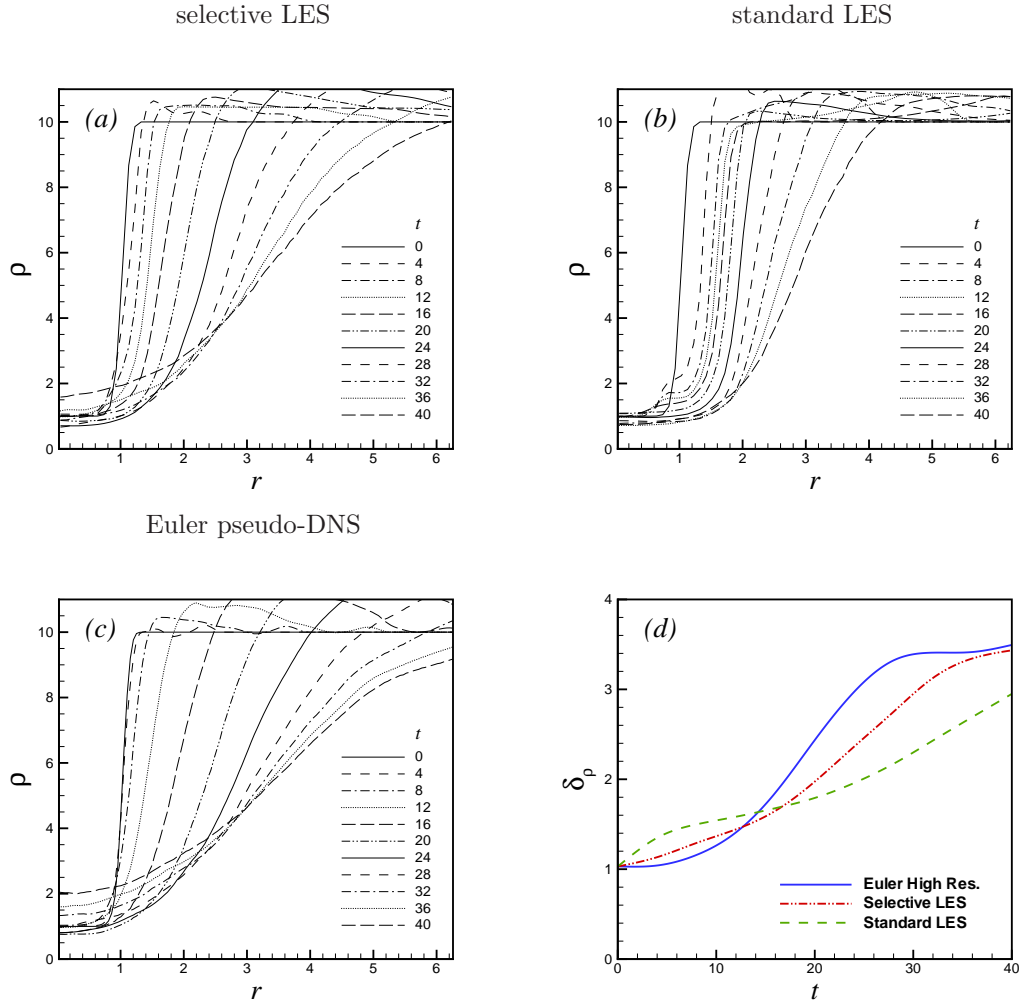


Figure 9: Time evolution of the mean density profiles and density thickness: (a) mean density, selective LES; (b) mean density, standard LES; (c) mean density, high resolution simulation, (d) density thickness  $\delta_\rho$ , evaluated as the distance from the jet axis where the mean density is the average between the jet axis density and the external ambient density. After the first 30 sound crossing times, the jet growth of the high resolution and selective LES simulations saturates the domain.

## References

- [1] D.Tordella, M.Iovieno, S.Massaglia, “Small scale localization in turbulent flows. A priori tests applied to a possible Large Eddy Simulation of compressible turbulent flows”, *Comp. Phys. Comm.* **176**(8), 539-549 (2007).
- [2] D.K.Lilly “The representation of small-scale turbulence in numerical simulation experiments”, *Proc. IBM Scientific Computing Symp. on Environmental Sciences*, Yorktown Heights, New York, ed. H.H. Goldstine, IBM form no. 320-1951 (1967).
- [3] V.M.Canuto, Y.Cheng, “Determination of the Smagorinsky–Lilly constant  $C_s$ ”, *Phys. Fluids* **9**(5), 13681378 (1997).
- [4] L.Biferale, G.Boffetta, A.Celani, A.Lanotte, F.Toschi, “Particle trapping in three-dimensional fully developed turbulence”, *Phys. Fluids*. **17**(2), 021701/1-4 (2005).
- [5] M.V.Morkovin, “Effects of compressibility on turbulent flows”, in *Mécanique de la turbulence*, edited by A. Favre, 367, (1961).
- [6] G.L.Brown, A.Roshko, “On density effects and large structure in turbulent mixing layers”, *J. fluid Mech.* **64**, 775–816, (1974).
- [7] C.Pantano, S.Sarkar, “A study in compressibility effects in the high-speed shear flows using direct simulations”, *J.Fluid Mech.*,**451**, 329–371 (2002).
- [8] M.Germano, U.Piomelli, P.Moin, W.H.Cabot, “A dynamic subgrid-scale eddy viscosity model”, *Phys. Fluids A* **3**, 1760, (1991).
- [9] A.W.Vreman, “An eddy-viscosity subgrid-scale model for turbulence shear flow: algebraic theory and applications”, *Phys. Fluids* **16**, 3670–3681, (2004).
- [10] S.Stolz, N.A.Adams, L.Kleiser, “The approximate deconvolution model for the large-eddy simulation of compressible flows and its application to shock-turbulent boundary layer interaction”, *Phys.Fluids* **10**, 2985–3001, (2001).
- [11] F.Ducros, P.Comte, M.Lesieur “Large-eddy simulation of transition to turbulence in a boundary layer developing spatially over a flat plate”, *J. Fluid Mech.* **326**, 1-36 (1996).
- [12] A.Mignone, G.Bodo , S.Massaglia, T.Matsakos, O.Tesileanu, C.Zanni and A.Ferrari, “PLUTO: a numerical code for computational astrophysics”, *Astr. J. Supplement Series* **170**(1), 228-242 (2007), and <http://plutocode.to.astro.it>.
- [13] P.Colella, P.R.Woodward, “The piecewise parabolic method (PPM) for gas-dynamical simulations, *J. comp. Phys.* **54**(1), 174–201, (1984).
- [14] F.Ducros, V.Ferrand, F.Nicoud, C.Weber, D.Darraq, C.Gacherieu, T.Poinsot, “Large-eddy simulation of the high-turbulence interaction”, *J. Comp. Phys.* **150**, 199–238, (1999).
- [15] G.Bodo, P.Rossi, S.Massaglia, “Three-dimensional simulations of jets ”, *Astron. & Astrophys.* **333**, 1117-1129 (1998).
- [16] M. Micono, G. Bodo, S. Massaglia, P. Rossi, A. Ferrari, R. Rosner, “Kelvin-Helmholtz Instabilities in Three Dimensional Radiative Jets”, *Astron. & Astrophys.*, **360**, 795-808 (2000).
- [17] D.Tordella, M.Belan, S.Massaglia, S.De Ponte, A.Mignone, E.Bodenschatz, A.Ferrari, “Astrophysical jets: insights into long-term hydrodynamics”, *New Journal of Physics* **13**, 043011 (2011).